Revisiting phase transformation mechanisms in LiNi$_{0.5}$Mn$_{1.5}$O$_4$ high voltage cathodes with operando microdiffraction

Isaac Martens,[†] Nikita Vostrov,[†] Marta Mirolo,[†] Mattia Colalongo,[†] Peter Kus,[‡] Marie-Ingrid Richard,[†,¶] Lianzhou Wang,[§] Xiaobo Zhu,[‖] Tobias U. Schulli,[*,†] and Jakub Drnec[*,†]

†European Synchrotron Radiation Facility, 71 Avenue des Martyrs, Grenoble 38000, France
‡Charles University, Faculty of Mathematics and Physics,Department of Surface and Plasma Science,V Holesovickach 2, 180 00 Prague 8, Czech Republic
¶Univ. Grenoble Alpes, CEA Grenoble, IRIG, MEM, NRS, 17 rue des Martyrs 38000 Grenoble, France
§Nanomaterials Centre, School of Chemical Engineering, and Australian Institute of Bioengineering and Nanotechnology, University of Queensland, QLD 4072 Australia
‖College of Materials Science and Engineering, Changsha University of Science and Technology, Changsha 410114, China

E-mail: schulli@esrf.fr; drnec@esrf.fr

Abstract

Understanding the phase transition mechanisms of active materials inside Li-ion batteries is critical for rechargability and optimizing the power/energy density of devices. In this work, high-energy microfocused X-ray diffraction is used to measure *in operando* the state-of-charge heterogeneities inside a high-voltage spinel (LiMn$_{1.5}$Ni$_{0.5}$O$_4$, LMNO) cathode. The structure of active material which resists complete delithiation is studied, towards unlocking the full storage capacity of ion-conductive spinels. High-precision diffraction also reveals nonlinear coupling between strain and lithiation state inside the cathode at high voltages, which suggests the phase diagram of this material is more complex than previously assumed. X-ray diffraction depth-profiling shows that large lithiation heterogeneities through the cross-section of the electrode are formed even at low currents, and that decoupling these gradients are necessary to study the phase transitions in detail.

Abbreviations

XRD, SOC, LMNO

Keywords

Li-ion batteries, high voltage cathode, LMNO, spinel, phase transition, lithiation

Introduction

Higher performance Li-ion battery electrodes are required for the next-generation of fast-charging and high power devices.[1] LiMn$_{1.5}$Ni$_{0.5}$O$_4$ (LMNO) is an advanced cathode active material, promising for battery electric vehicle applications due to its high voltage at all states-of-charge, Co-free and Ni-poor

formula, and relatively stable crystal framework.[2–4] In addition, LMNO is capable of high rate (dis)charge capability, even at large particle sizes due to the spinel structure's excellent Li ion conductivity with 3D diffusion pathways.[5,6]

Utilization of LMNO is hindered by two key issues. The first problem is instability at high potential in conventional electrolytes, which causes transition metal leaching,[7,8] self-discharge,[9] and irreversible capacity loss.[10] The second problem is that LMNO has a deceptively complex microstructure and phase diagram.[11,12] The (de)lithiation mechanism and kinetics are strongly influenced by the presence of Mn/Ni ordering,[13,14] Mn^{3+} content,[15,16] antiphase domains,[17] oxygen vacancies,[18,19] surface faceting,[9,18] surface-localized impurities,[7,20] cycling history,[18] cycling rate,[21] annealing history,[12,22] temperature[23] and doping.[24] The difficulty in controlling or even measuring these structural parameters prevents the preparation of well-defined material, and has led to inconsistent results across the literature.[11] Furthermore, these microstructural motifs usually co-exist inside the same material and are coupled to one another, which complicates mechanistic understanding.[16,22]

Consensus has emerged on several aspects of lithiation mechanics: LMNO possesses at least three thermodynamically stable phases: the fully lithiated $LiMn_{1.5}Ni_{0.5}O_4$ (Li_1, Ni^{2+}), the half-lithiated $Li_{0.5}Mn_{1.5}Ni_{0.5}O_4$ ($Li_{0.5}$, Ni^{3+}), and the fully delithiated $Mn_{1.5}Ni_{0.5}O_4$ (Li_0, Ni^{4+}).[25–27] The first phase transition from Li_1 to $Li_{0.5}$ occurs during the first voltage plateau of the charging curve (4.7 V) initially through a solid-solution mechanism, which switches to a phase-segregation mechanism.[21] The second phase transition from $Li_{0.5}$ to Li_0 occurs during the second voltage plateau (4.75 V), mostly through a phase segregated mechanism with a small solid-solution component.

One major objective is to understand and maximize the solid-solution behavior between these three states during operation, since sharp phase segregation is well-known to slow down kinetics and accelerate degradation.[22,28] Significant variations in the competition of the solid-solution vs phase segregation mechanisms during both phase transitions have been reported by many groups. This has led to contradictory mechanisms being proposed including single-phase,[18,29] two-phase,[21,23,30] and even three phase[16,27] coexistence inside individual crystals. The relatively flat voltage curve of LMNO places all of these states very close in energy, which makes experimentally probing the phase diagram difficult. Only a few operando X-ray or neutron diffraction studies with very high quality intensity, time, and angular resolution exist.[20,21,31,32]

It is challenging to reconcile the high Li mobility with the practical observation that it is difficult to electrochemically extract all of the Li from the lattice of many spinel oxides, which limits the practical energy storage capacity of these materials.[33,34] The usable specific capacity of LMNO varies wildly across studies, ranging from less than half to above 98% of the theoretical $146\,\mathrm{mA\,h\,g^{-1}}$, typically around 90%.[35] While a 10% fraction of "redox-inactive" material is sometimes observed in LMNO, the presence of this phase is rarely acknowledged, and is challenging to explain.[16,20,25,31,36] Rapid and/or deep delithiation has also been shown to induce cracking and fracturing of large LMNO crystals, which degrades device performance.[27] These numerous connections between the phase transitions with the capacity and durability of LMNO motivate an in-depth understanding of the lithiation mechanism.

X-ray diffraction (XRD) depth profiling is an emerging technique for investigating state-of-charge (SOC) gradients through the plane of electrodes.[37] During (de)lithiation, limited electronic and ionic conductivity through electrodes, as well as the fundamental intercalation kinetics of active material, produce substantial heterogeneity through the thickness of electrode films.[37,38] While these effects are obviously accentuated at extreme current densities, a growing body of evidence supports the existence and importance of gradients during lower C-rate operation.[39] The small number of time, potential, and depth resolved in situ studies limits the scope of our understanding of electrode SOC heterogeneity.[40] Because

the rate capability of conventional lithium-ion cells is normally limited by the graphite anode, a large percentage of these studies have focused on enabling faster charging of anode active materials,[37,38,41,42] while a comparatively fewer number have considered cathode SOC heterogeneity.[40,43] In highly conductive oxides like LMNO, SOC heterogeneity can be governed not by the active material, but by concentration gradients in the electrolyte. A clear picture of these SOC gradients inside practical electrodes are needed to deconvolute simple transport phenomena from fundamental lithation kinetics, and model the rate limitations of next-generation cathodes from individual crystallites to the cell level.

In this work, we use high-speed X-ray microdiffraction to enable deeper understanding of LMNO cathode solid-state chemistry at the inter and intraparticle scale. SOC gradients are observed even when cycling at a modest current density of $16\,\mu\mathrm{A\,cm^{-2}}$, equivalent to a cycling rate of C/6 (one full charge in 6 hours). Substantial kinetic limitations in both phase transitions are observed, for charging and discharging directions. Our approach enables the (inter-particle) ionic conductivity through the electrode to be decoupled from the (intra-particle) ionic conductivity through the lattice of the active material, providing a clearer picture of what limits the rate capability and accessible capacity in advanced cathode materials inside functional electrodes. The unprecedented signal quality enabled by fourth-generation synchrotrons,[44] reveals a small but quantifiable fraction of electrochemically active LMNO which resists complete delithiation, raising further questions about the complex phase transition mechanisms, and its link to the cation kinetics, inside these cathodes.

Results and discussion

In situ synchrotron powder diffraction was collected over the first charge-discharge cycle of a Swagelok-geometry LMNO/Li cell at a rate of C/6. A constant-current/constant-voltage (CC-CV) profile was used to understand the dynamics at high potentials.

Powder diffraction acquired from the middle of the cathode film's cross-section during the cycle is presented in Figure 1. Diffraction from the as-prepared electrode and its analysis is provided in the supplementary material (Figs. S3 and S7), which matches the data from the initial assembled cell, showing that the cell assembly and contact with the electrolyte does not induce major structural modifications. Because of the cubic symmetry of spinel LMNO, all XRD reflections show the same proportionate shift as a function of potential, but those at higher angle are sampled with better resolution in reciprocal space. Therefore, we focus our analysis on the 531 reflection ($4.54\,\mathrm{\AA}^{-1}$ to $4.66\,\mathrm{\AA}^{-1}$), which does not significantly overlap with any intense neighbouring reflections. The trends observed are qualitatively in agreement with many previous reports of *in situ* XRD on LMNO.[18,27,29,32,43] These changes are roughly symmetrical upon discharge, with a small hysteresis detected in the peak position.

Incomplete delithiation

The exceptional quality of the diffraction data provided by the new Extremely Brilliant Source at the European Synchrotron[44] allows for fully quantitative analysis of weak, higher order reflections from minor phases in less than 1 s exposures in a microfocused beam. This unprecedented sensitivity combined with narrower natural linewidths at high angles permits the differences between the first and second phase transition to be fully resolved, along with the intermediates formed during those processes.

Interestingly, we found that a small quantity of LMNO does not completely delithiate (Fig. 2A). After being held at 5.0 V for 1 hour, 6.5% of the $\mathrm{Li_1}$ phase and 3.5% of the $\mathrm{Li_{0.5}}$ phase remain, while 90.0% of the LMNO is converted to the $\mathrm{Li_0}$ phase (Fig. 2B). It is foreseeable that some small fraction of the LMNO is electrically isolated in the electrode, and would therefore not participate in the phase transitions. However, this cannot explain the fraction of LMNO which undergoes the first phase transition at 4.72 V to $\mathrm{Li_{0.5}}$ but becomes trapped in this in-
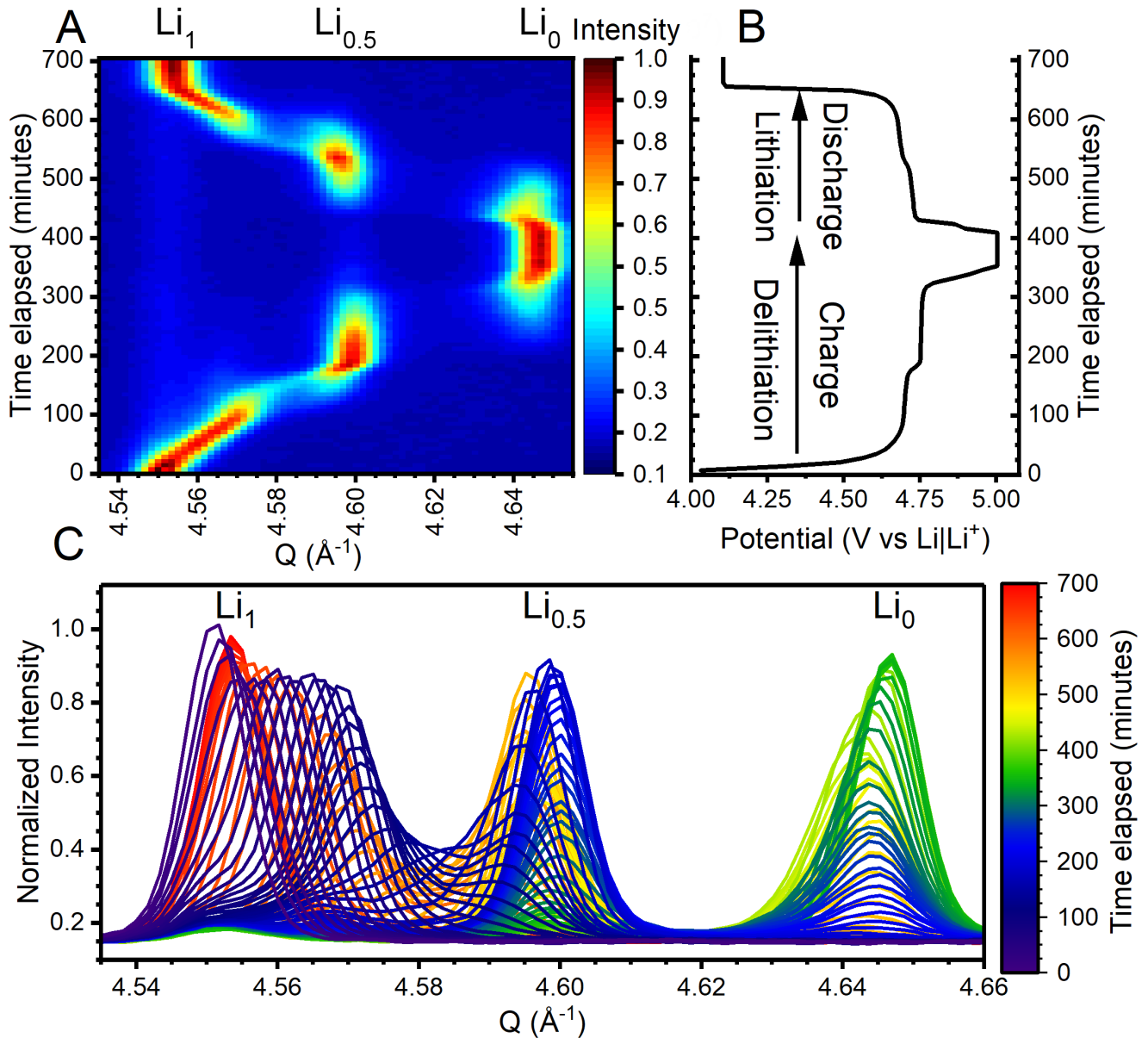
Figure 1: Powder diffraction of the LMNO 531 reflection over the course of a charge-discharge cycle, recorded from the middle of the electrode. Waterfall plot of the normalized intensities of the Li_1, $Li_0.5$, and Li_0 peaks (A). Charging curve of the operando cell during measurement using a constant current-constant voltage (CC-CV) protocol up to 5.0 V (B). Overlaid patterns of the 531 reflection shown in part A. Every tenth powder pattern recorded is plotted here. (C).

termediate state, even when held at 5 V. This $Li_{0.5}$ phase disappears again during the discharge, indicating that those particles remain electrically/ionically connected throughout cycling, but are somehow unable to completely delithiate. The low charging rate (C/6), and long hold at very high potentials (1 hour at 5 V) applied here preclude any other ionic or electronic conductivity effects from limiting the phase transitions.

Many groups have repeatedly noted the difficulty of extracting more than around 90% of the the Li ions from spinel active materials based on electrochemical and Li stoichiometry measurements.[19,21,33,34,45] In an extreme case, Kan *et al.* showed that a carefully annealed LMNO had dramatically lowered capacity, where less than 20% of the Li was capable of being extracted in the first cycle, and with the capacity gradually increasing on subsequent cy-
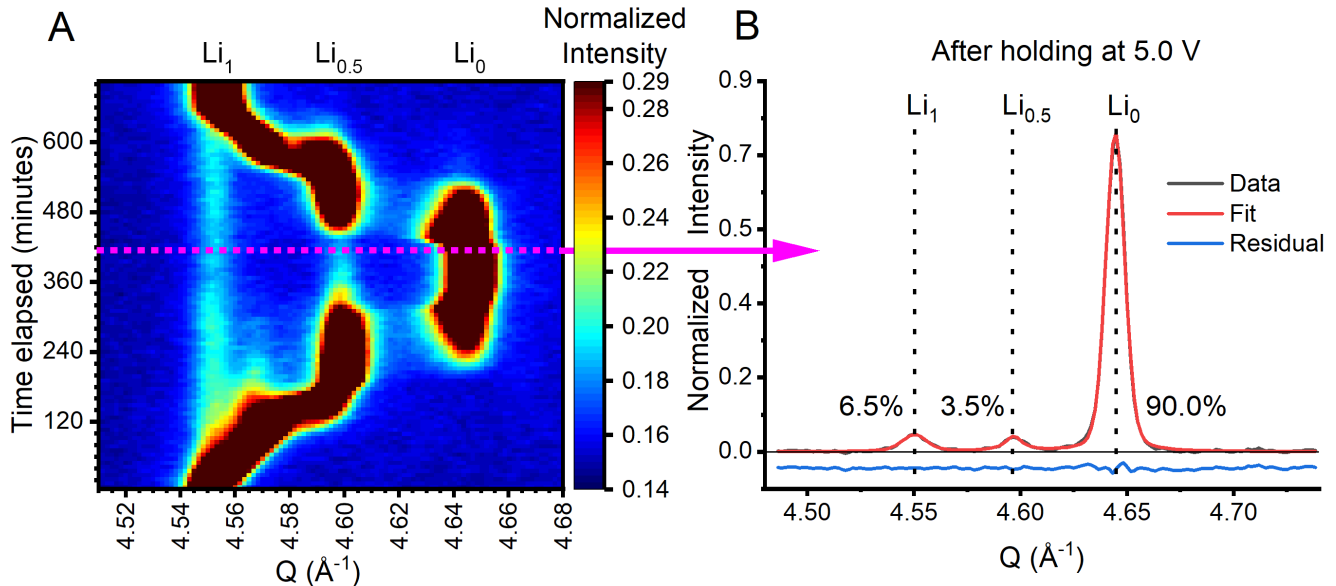
Figure 2: Waterfall plot of the diffraction intensities of the Li_1, $Li_0.5$, and Li_0 peaks for the LMNO 531 reflection, with contrast adjusted to show the trace quantities of the inactive phases.(A) Powder diffraction after 1 hour hold at 5.0 V (B, extracted from magenta line in A). Each of the Li_1, $Li_{0.5}$, and Li_1 phases were background subtracted, fit with pseudo-Voight lineshapes, and integrated.

cles.[18] However, several *in situ* diffraction studies on LMNO do not observe any untransformed phases, despite having a detection limit sufficient to observe them.[21,29,32] These contradictory results may be attributed to differences in the crystal morphology, crystal quality, crystallite size, pre-cycling, and charging rate of the LMNO used in each study, which lead to substantial differences in solid state reactivity.[46]

One of the possible explanations is that some small fraction of LMNO crystallites experience strong heterogeneity in lithiation, with large barriers to phase transitions. This has been discussed by Bauer et al. when they detected that ca. 10% of the Ni^{3+} and Mn^{3+} in LMNO was not fully oxidized at 5 V, similar to this work, using *operando* XANES mapping.[26] Their imaging further revealed that these unoxidized regions are concentrated in specific particles. Unfortunately overlap between particles prevented understanding whether these SOC gradients occur only at the interparticle scale, or also inside individual crystallites. However, persistent intra-particle state of charge heterogeneity has been observed in several cathode active materials.[47] These states likely also exist in charged LMNO, since they are known to occur in both the pristine, fully lithated starting material[48,49] and in chemically delithiated samples.[27]

Additionally, differences in phase transition kinetics have often been attributed to the formation of lower-symmetry phases of LMNO, where the occupancies of Ni and Mn inside the lattice are not randomly distributed, but locally structured.[50,51] The LMNO in this work was not subjected to long annealing at high temperature and slow cooling which is necessary to produce cation ordering. Analysis of the active material scraped from fresh electrodes exhibited no extra superstructural reflections characteristic of these phases, and only a trace quantity of rock-salt impurity (Fig. S8). Control experiments on annealed LMNO indicated that even very small quantities of ordering are detectable with synchrotron diffraction (<0.1 wt%). Therefore, it is reasonable to conclude that ordered Mn/Ni domains are not responsible for the incomplete delithiation.

The presence of antisite defects (Ni-Li site swapping) have also been suggested to inhibit LMNO phase transition kinetics.[50] We checked this hypothesis by analyzing the weak 220 reflection which draws most of its scattering

5

power from the Li lattice position. Its quantitative disappearance during delithiation indicates no detectable Ni in this site, and therefore no substantial quantity of antisite defects inside the LMNO (Fig. S7).

LMNO is known for having 3D Li-ion conduction pathways and very fast intrinsic rate capability, therefore this incomplete delithiation behavior is unexpected. Even though we do not have a definite answer for the observed incomplete delithiation, we suggest that defects, mosaicity, and coherency strain inside large single crystals are responsible, as these can locally disrupt ion conduction, creating pinned states and energy barriers to phase transitions.[20,52] Furthermore, large strain gradients inside crystals can lead to cracking, enhanced corrosion, and degradation processes.[48] We believe that future understanding of these apparent barriers to phase transformation is critical to unlock the full theoretical capacity, charging rate, and durability of these high voltage active materials, toward batteries with longer lifetimes, and higher energy/power densities.

Solid solutions at high potentials

Understanding these degradation processses in LMNO at high potentials requires a precise understanding of which phases are formed under these conditions. The relatively high temporal and angular resolution of the diffraction data allows for precise measurements of the solubility of the different phases into solid solutions. While the $Li_{0.5}/Li_0$ phase transition is often suggested to follow an exclusively phase segregated mechanism, it is clear from Figure 1A and C that a significant evolution of the Li_0 peak width and position occurs.[53] A completely phase-segregated mechanism with rapid Li diffusion would show no evolution in lattice parameter (peak position), and only changes in intensity and crystallite size (peak shape) of two peaks would be observed. These shifts, occuring for both lithiation and delithiation, were probed by peak fitting of the 622 reflection from the Li_0 phase over the course of the charge-discharge cycle (Figure 3). A green arrow marks the end of the second voltage plateau.

Red, blue, and magenta lines have been added as a guide for the eye, and correspond to the onset points of the 5.0 V hold, a brief period of cell relaxation, and the discharge respectively. This fitting was performed on the same data shown in Figures 1 and 2. A full Rietveld analysis of all three phases including the mixed-phase regime at lower potentials is severely compromised by the peak overlap of the different metastable solid-solution intermediates, which has been discussed elsewhere.[21]

Rietveld refinement of the pristine material indicated that the crystallite size of the Li_1 phase was immeasurably large at all time points (> 100 nm), and that all of the measurable peak broadening corresponds to local distortion of the lattice parameter in the crystals, commonly referred to as microstrain. Microstrain broadening can be interpreted here as the ordering of Li inside the lattice, and the degree to which microscopic Li occupancy varies inside the Li_0 domains. The constant peak width and stable or slowly decreasing lattice parameter of the Li_0 phase during the second charging plateau (below 4.77 V) indicates that at these potentials, the $Li_{0.5}$ phase is slowly turning into Li_0 domains and it is energetically favorable to keep these domains in a highly disordered, moderately strained state. At or below this potential, the Li stoichiometry of the slowly growing Li_0 domains and the Li ordering inside them are effectively constant, although the quantity of this phase steadily increases.

After reaching a potential of 4.76 V (330 minutes, green arrow), the potential begins to increase steeply (Fig. 3A). Concurrent with the potential increase, the peak position of the Li_0 phase also begins to increase (Fig. 3B, green arrow). Removing the last few percent of Li^+ ions becomes progressively more difficult, and creates extra strain in the lattice. The peak width also begins to decrease, indicating that the variation in Li occupancy is reduced and the domains are becoming more ordered. At 4.76 V the Li_0 phase intensity has only reached around 50% of the maximum value (Fig. 3C, green arrow).

The Li stoichiometry in the Li_0 solid solution can be estimated by linear interpolation of

the peak shifts.[21] Using this method, the point where the cell potential and peak position begins to increase corresponds to a composition of $Li_{0.03}$ in the Li_0 phase. (Figs. 3A and B, green arrows). This is close to the concentration of Mn^{3+} in this sample (3.9%, Fig. S3). Therefore, we attribute this peak shift at high potentials to either the onset of repulsive interactions in the lattice as the occupancy of Li decreases, or to an additional energy barrier associated with removing Li nearby Mn^{3+} defects in the lattice.

The Li_0 intensity begins to plateau at 4.879 V after reaching 83% of its maximum, with a gradual small increase while the potential is held for 1 hour at 5.0 V (Fig. 3C). Conversely, the lattice parameter and peak width continue to evolve until 5.0 V is reached (the red vertical line), and then remain relatively constant (Fig. 3B and D). After the potential hold, the cell was allowed to relax for 15 minutes (between the blue and magenta lines). During the relaxation phase, the potential and lattice parameter immediately begin to decrease, and the intensity and peak width remain constant. While the voltage decay is a convolution of electrochemical kinetics, Li^+ concentration gradients, and depolarizing reactions, any evolution in the diffraction signal must reflect structural re-lithiation, and can therefore be assigned to self-discharge. Because the peak position shifts, while the intensity and widths do not, we can infer that the Li ions rapidly re-insert and equilibrate throughout the crystals on the time scale of seconds during relaxation, and that any surface layers formed at high potentials do not dramatically impede the Li conductivity.

Once the discharge is initiated (magenta line) the peak intensity begins to reduce, while the peak width broadens. The diffraction shows the process is partially symmetrical upon discharge, with the lattice parameter reaching a minimum at 4.732 V (463 minutes), where the intensity of the L_0 is 62%.

Simple solid solution behavior predicts linear shifts in peak position and intensity. The strongly nonlinear behavior and mismatch between the lattice parameter, microstrain, and intensity between 4.879 V and 5.0 V must re-flect the continued structural ordering of the lattice and electrode-surface interactions,[46,54] independent of the growth of Li_0 domains. These reactions likely include an interplay of Mn valence, irreversible rock-salt impurities, electrolyte decomposition, oxygen vacancy formation, which are directly responsible for performance fade in full devices.[11] Although these effects have been detected *ex situ* in cycled crystals, we are not aware of any in-situ measurements of these high voltage and defect mediated transformations.[51,55] The instability of the electrolyte between 4.75-5.0 V prevents a comparative coulombmetric analysis in this window.

In light of our results, more work is clearly needed to understand the link between these Li^+ dynamics, and the reactions involved in self-discharge, which limits the practical application of LMNO and other high voltage cathode materials.

Depth profiling the state of charge

A major advantage of grazing incidence microbeam diffraction is that depth profiles through planar electrode films of conventional thickness can be obtained. Without depth-resolution, the influence of finite electronic/ionic conductivity limits the precision of mechanistic investigations, such as determining the miscibility of the different phases in solid solution. These SOC gradients create a distribution of material properties which are averaged through the thickness of the electrode in most studies, and therefore blurred together. Measuring this additional dimension of the electrode allows for these effects to be decoupled. In our experiments the beam was scanned through the cross section of the electrode with 5 µm resolution during the whole experiment.

Figure 4 shows the results of a Rietveld refined linescan collected near the end of the second voltage plateau (318 min elapsed, 4.755 V). A detectable SOC gradient can be observed through the depth profile of the electrode, using the relative peak intensities. The ratios of the $Li_{0.5}$ and Li_0 peak intensities show a clear trend, with the regions closer to the separator having a
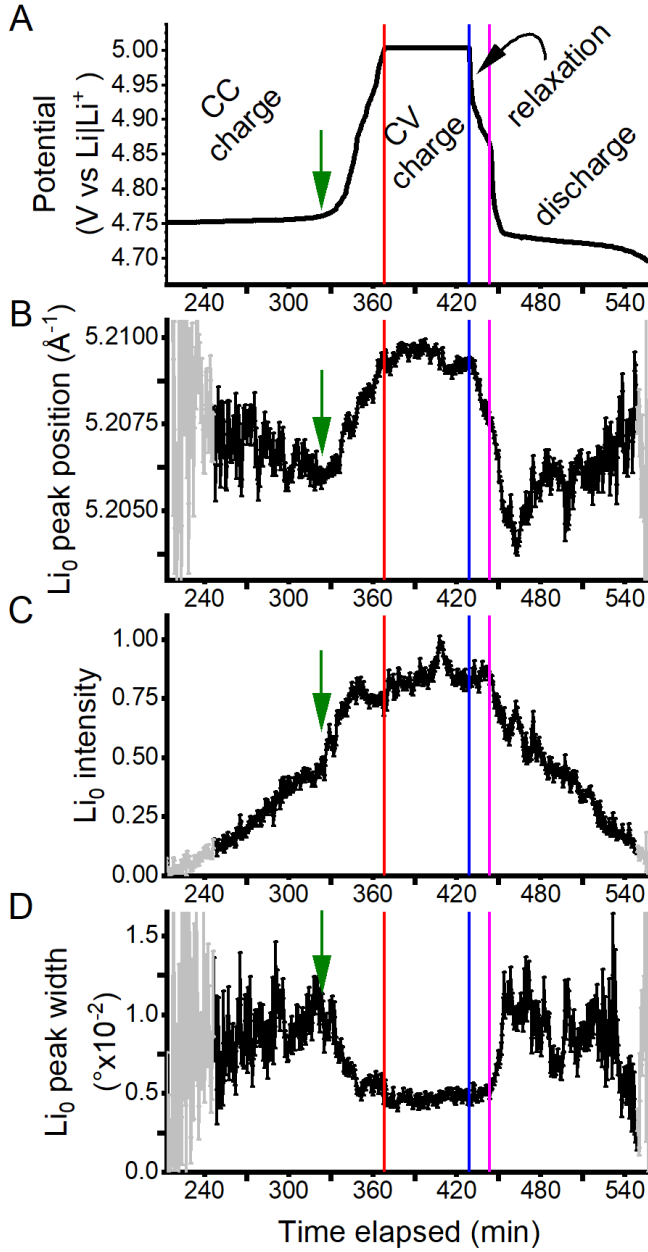
Figure 3: Rietveld refinement of the Li_0 phase at high state of charge, using the 622 reflection. Cell potential profile (A), peak position (B), normalized peak intensity (C), and peak width (D). The green arrow indicates the end of the second voltage plateau. Red, blue, and magenta lines correspond to the beginning of the 5.0 V hold, cell relaxation, and discharge respectively. Error bars are the standard deviation estimated from the Rietveld covariance. Points corresponding to less than 10% of the maximum phase intensity are colored in gray, and are noisier due to the low detected intensity.

lower ratio than the regions closer to the current collector on the right-hand side (Fig. 4). The magnitude of this depth profile effect is substantial, with the phase transition progressing 41% further in the region of the electrode closer to the separator.
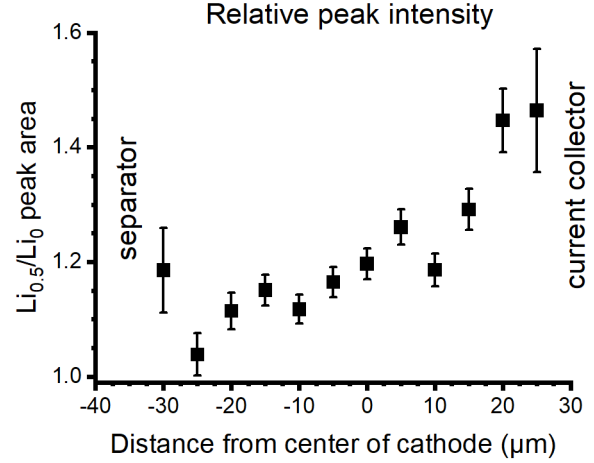

Figure 4: State of charge depth profile through the LMNO cathode at 4.755 V during charging. $Li_{0.5}$:Li_0 peak ratios calculated for the cross sectional linescan through the cathode, determined using the 531 reflection. The separator is on the left side, while the current collector is on the right side of the cathode. Error bars represent the standard deviation estimated from the Rietveld covariance matrix.

Because the SOC is higher further away from the current collector during the charging, it can be rationalized that the ionic, and not the electronic conductivity of the electrode is producing the through-plane lithiation gradient in this experiment.[39] Since these gradients are observed in a cell using a conventional Li-ion electrolyte, reasonably low C-rate, and "high-speed" active material, all of which suppress SOC gradients, it is concluded that through-plane SOC heterogeneity is likely a very common phenomena in standard Li-ion electrodes, even though it is rarely measured.[20,56] Imaging the gradients formed inside electrodes is itself important for optimizing battery coatings, and power performance.[37–39,56]

After the X-ray experiment, continued *ex situ* cycling of the cell demonstrated equivalent performance as during beam exposure, with grad-

ual capacity fade as expected during cycling to very high potentials (Fig. S2). *Operando* experiments over a larger number of cycles are necessary to probe how phase transitions contribute to the mechanisms of irreversible capacity loss.[10]

Conclusions

Advances in *operando* X-ray diffraction allow easy access to the fine structure of active materials which have previously only been visible using neutron scattering, but now with much higher spatiotemporal resolution. Details of the phase transition mechanisms inside high-voltage cathode materials such as LMNO are required to accelerate their commercialization, since these processes are directly responsible for their capacity, durability, and rate performance.

Trapped, lithiated LMNO phases linked to the complicated phase transition kinetics inside ion-conductive spinels were clearly quantified for the first time. These trapped states limit ion (de)intercalation and partly explain the diversity in reported LMNO capacities, although their physical origin remains poorly understood.

High speed, precision measurements of the LMNO lattice parameter during deep delithiation show unusual nonlinear strain evolution associated with active material degradation processes, and provide a way to quantify rapid self-discharge reactions.

Depth-profile microdiffraction demonstrates that large state-of-charge gradients are established through the plane of the electrode, even under conditions which are typically thought to minimize these effects, such as high-conductivity electrolyte, low C-rate, high speed active material, and thin electrode coatings. Decoupling this heterogeneity at the electrode scale from the crystallite scale is necessary to differentiate phase transition mechanisms, and to optimize electronic and ionic conductivity inside electrode films.

Unravelling the phase transition mechanisms inside LMNO will ultimately require a better understanding of heterogeneities at the single-particle level.[20,21,27,57] Nanofocused X-ray beams are well-suited to probe the complex microstructure inside cathode active materials,[48] and the rapid advances in this field are likely to provide even deeper insight.

Materials and Methods

The LMNO active material was synthesized using high temperature solid state synthesis as described elsewhere.[10] The disordered phase was prepared by annealing at $750\,°C$ for 10 hours, then cooling at $2\,°\mathrm{min}^{-1}$ An ink was prepared with a composition of 85 wt % LMNO, 10 wt % conductive carbon, and 5 wt % polyvinylidene fluoride as a binder. The ink was coated onto Al foil using a doctor blade, producing electrodes with areal capacity of $0.136\,\mathrm{mA\,h\,cm}^{-2}$, measured using slow cycling up to $4.85\,V$. Direct measurements of the active material mass loading on small electrodes were less accurate, but was approximately $1.4\,\mathrm{mg\,cm}^{-2}$, corresponding to an experimental Li capacity of $102\,\mathrm{mA\,h\,g}^{-1}$. The powder diffraction experiment determined the utilization and electrical connectivity of the active material was a minimum of 93.5%. The charging curves in the main text are presented over time because of uncertainties in the current efficiency at high potential and the areal mass loading, as well as the poorly defined total Li capacity of the LMNO material. Charge-discharge curves as a function of cell capacity and differential coulometry are available in the Supporting Information (Fig. S3).

A commercial, 0.25 inch diameter "Swagelok"-style[58] half cell was used for the diffraction experiment (S4R, France). The perfluoroalkoxy polymer body was lathed to a wall thickness of approximately $200\,\mu m$ to minimize scattering from the cell body (Fig. S1). A relatively thick glass fiber separator (EL-CELL, 1 mm) was used to create gentle homogeneous compression of the stack during operation. Li foil (99.9% purity, 0.75 mm thickness, VWR), was used as a counterelectrode. The electrolyte was 20 uL of 1.0 M $LiPF_6$ in ethylene carbonate/ethyl methyl carbonate (3/7 g/g, LP-57), added in several portions to the separator to

ensure a fully wetted cell. A Biologic SP-240 potentiostat was used to control the cell potential.

Operando powder diffraction was collected at ESRF beamline ID31. The X-ray wavelength was 0.161 Å (77 keV), and the cathode was selectively illuminated at grazing incidence with a beam 25x5 µm in horizontal x vertical size. The data was collected using a Pilatus 2M CdTe detector at a distance of 2.25 m using an exposure time of 1 s per pattern, measured every 30 s with an incident flux of 6×10^{10} ph/s. Data was radially integrated using the PyFAI analysis package, calibrated with NIST SRM 674b CeO_2.

For the analysis of the 531 reflection shown in Fig. 4, the integrated peak intensities of each phase were weighted to account for the small change in structure factor upon delithiation, calculated using VESTA 3.57.

The relatively high flux density of the X-ray beam used in this work could perturb the local potential inside active cells. To determine the extent of undesirable beam influence, a separate control experiment was performed where two different spots on an LMNO electrode inside the operando cell were given different X-ray doses while cycling. The first location was given a dose equivalent to that shown in this work, while the second location was given a 10-fold higher dose. The phase transitions of the LMNO were unaffected by changes in the beam dose, leading us to conclude that exposure in this range does not produce substantial X-ray damage, at least over one cycle. High energy X-rays such as those used in this work have previously been shown to minimize or eliminate beam damage during cycling, versus lower energies which are more strongly absorbed.[59]

Supporting Information Available

Details regarding the electrochemical cycling, powder diffraction patterns, and electron microscopy imaging, are available in Supporting Information file.

References

1. Wu, F.; Maier, J.; Yu, Y. Guidelines and trends for next-generation rechargeable lithium and lithium-ion batteries. *Chemical Society Reviews* **2020**, *49*, 1569–1614.

2. Zhong, Q.; Bonakdarpour, A.; Zhang, M.; Gao, Y.; Dahn, J. R. Synthesis and Electrochemistry of LiNi x Mn2 - x O 4. *Journal of The Electrochemical Society* **1997**, *144*, 205–213.

3. Zhao, H.; Lam, W.-Y. A.; Sheng, L.; Wang, L.; Bai, P.; Yang, Y.; Ren, D.; Xu, H.; He, X. Cobalt-Free Cathode Materials: Families and their Prospects. *Advanced Energy Materials* **2022**, *12*, 2103894.

4. Liang, G.; Peterson, V. K.; See, K. W.; Guo, Z.; Pang, W. K. Developing High-Voltage Spinel LiNi0.5Mn1.5O4cathodes for High-Energy-Density Lithium-Ion Batteries: Current Achievements and Future Prospects. *Journal of Materials Chemistry A* **2020**, *8*, 15373–15398.

5. Xiao, J.; Chen, X.; Sushko, P. V.; Sushko, M. L.; Kovarik, L.; Feng, J.; Deng, Z.; Zheng, J.; Graff, G. L.; Nie, Z.; Choi, D.; Liu, J.; Zhang, J.-G.; Whittingham, M. S. High-Performance LiNi 0.5 Mn 1.5 O 4 Spinel Controlled by Mn 3+ Concentration and Site Disorder. *Advanced Materials* **2012**, *24*, 2109–2116.

6. Amin, R.; Belharouk, I. Part I: Electronic and ionic transport properties of the ordered and disordered LiNi0.5Mn1.5O4 spinel cathode. *Journal of Power Sources* **2017**, *348*, 311–317.

7. Lin, M.; Ben, L.; Sun, Y.; Wang, H.; Yang, Z.; Gu, L.; Yu, X.; Yang, X.-Q.; Zhao, H.; Yu, R.; Armand, M.; Huang, X. Insight into the Atomic Structure of High-Voltage Spinel LiNi $_{0.5}$ Mn $_{1.5}$ O $_4$ Cathode Material in the First Cycle. *Chemistry of Materials* **2015**, *27*, 292–303.

8. Gong, Y.; Chen, Y.; Zhang, Q.; Meng, F.; Shi, J.-A.; Liu, X.; Liu, X.; Zhang, J.; Wang, H.; Wang, J.; Yu, Q.; Zhang, Z.; Xu, Q.; Xiao, R.; Hu, Y.-S.; Gu, L.; Li, H.; Huang, X.; Chen, L. Three-dimensional atomic-scale observation of structural evolution of cathode material in a working all-solid-state battery. *Nature Communications* **2018**, *9*, 3341.

9. Kuppan, S.; Duncan, H.; Chen, G. Controlling side reactions and self-discharge in high-voltage spinel cathodes: the critical role of surface crystallographic facets. *Physical Chemistry Chemical Physics* **2015**, *17*, 26471–26481.

10. Zhu, X.; Schülli, T. U.; Yang, X.; Lin, T.; Hu, Y.; Cheng, N.; Fujii, H.; Ozawa, K.; Cowie, B.; Gu, Q.; Zhou, S.; Cheng, Z.; Du, Y.; Wang, L. Epitaxial growth of an atom-thin layer on a LiNi0.5Mn1.5O4 cathode for stable Li-ion battery cycling. *Nature Communications* **2022**, *13*.

11. Aktekin, B.; Valvo, M.; Smith, R. I.; Sørby, M. H.; Lodi Marzano, F.; Zipprich, W.; Brandell, D.; Edström, K.; Brant, W. R. Cation Ordering and Oxygen Release in LiNi 0.5– x Mn 1.5+ x O 4– y (LNMO): In Situ Neutron Diffraction and Performance in Li Ion Full Cells. *ACS Applied Energy Materials* **2019**, *2*, 3323–3335.

12. Saravanan, K.; Jarry, A.; Kostecki, R.; Chen, G. A study of room-temperature LixMn1.5Ni0.5O4 solid solutions. *Scientific Reports* **2015**, *5*, 8027.

13. Lee, E.; Persson, K. A. Solid-Solution Li Intercalation as a Function of Cation Order/Disorder in the High-Voltage Li $_x$ Ni $_{0.5}$ Mn $_{1.5}$ O $_4$ Spinel. *Chemistry of Materials* **2013**, *25*, 2885–2889.

14. Kim, J.-H.; Huq, A.; Chi, M.; Pieczonka, N. P.; Lee, E.; Bridges, C. A.; Tessema, M. M.; Manthiram, A.; Persson, K. A.; Powell, B. R. Integrated Nano-Domains of Disordered and Ordered Spinel Phases in LiNi $_{0.5}$ Mn $_{1.5}$ O $_4$ for Li-Ion Batteries. *Chemistry of Materials* **2014**, *26*, 4377–4386.

15. Cabana, J.; Casas-Cabanas, M.; Omenya, F. O.; Chernova, N. A.; Zeng, D.; Whittingham, M. S.; Grey, C. P. Composition-structure relationships in the li-ion battery electrode material LiNi0.5Mn1.5O4e. *Chemistry of Materials* **2012**, *24*, 2952–2964.

16. Duncan, H.; Hai, B.; Leskes, M.; Grey, C. P.; Chen, G. Relationships between Mn $^{3+}$ Content, Structural Ordering, Phase Transformation, and Kinetic Properties in LiNi $_x$ Mn $_{2-x}$ O $_4$ Cathode Materials. *Chemistry of Materials* **2014**, *26*, 5374–5382.

17. Casas-Cabanas, M.; Kim, C.; Rodríguez-Carvajal, J.; Cabana, J. Atomic defects during ordering transitions in LiNi $_{0.5}$ Mn $_{1.5}$ O $_4$ and their relationship with electrochemical properties. *Journal of Materials Chemistry A* **2016**, *4*, 8255–8262.

18. Kan, W. H.; Kuppan, S.; Cheng, L.; Doeff, M.; Nanda, J.; Huq, A.; Chen, G. Crystal Chemistry and Electrochemistry of LixMn1.5Ni0.5O4 Solid Solution Cathode Materials. *Chemistry of Materials* **2017**, *29*, 6818–6828.

19. Niemöller, A.; Jakes, P.; Eurich, S.; Paulus, A.; Kungl, H.; Eichel, R.-A.; Granwehr, J. Monitoring local redox processes in LiNi 0.5 Mn 1.5 O 4 battery cathode material by in operando EPR spectroscopy. *The Journal of Chemical Physics* **2018**, *148*, 014705.

20. Singer, A.; Ulvestad, A.; Cho, H. M.; Kim, J. W.; Maser, J.; Harder, R.;

Meng, Y. S.; Shpyrko, O. G. Nonequilibrium structural dynamics of nanoparticles in $LiNi_{1/2}Mn_{3/2}O_4$ cathode under operando conditions. *Nano Letters* **2014**, *14*, 5295–5300.

21. Komatsu, H.; Arai, H.; Koyama, Y.; Sato, K.; Kato, T.; Yoshida, R.; Murayama, H.; Takahashi, I.; Orikasa, Y.; Fukuda, K.; Hirayama, T.; Ikuhara, Y.; Ukyo, Y.; Uchimoto, Y.; Ogumi, Z. Solid Solution Domains at Phase Transition Front of LixNi0.5Mn1.5O4. *Advanced Energy Materials* **2015**, *5*, 1500638.

22. Moorhead-Rosenberg, Z.; Huq, A.; Goodenough, J. B.; Manthiram, A. Electronic and Electrochemical Properties of $Li_{1-x}Mn_{1.5}Ni_{0.5}O_4$ Spinel Cathodes As a Function of Lithium Content and Cation Ordering. *Chemistry of Materials* **2015**, *27*, 6934–6945.

23. Takahashi, I.; Murayama, H.; Sato, K.; Naka, T.; Kitada, K.; Fukuda, K.; Koyama, Y.; Arai, H.; Matsubara, E.; Uchimoto, Y.; Ogumi, Z. Kinetically asymmetric charge and discharge behavior of $LiNi_{0.5}Mn_{1.5}O_4$ at low temperature observed by in situ X-ray diffraction. *J. Mater. Chem. A* **2014**, *2*, 15414–15419.

24. Li, J.; Wang, H.; Dong, W.; Shi, Z.; Xie, W.; Qiao, H.; Yu, Q.; Zhang, M.; Hu, J.; Yang, L.; Hong, J. Phase Transition Dominated High-Rate Performances of the High Voltage $LiNi_{0.5}Mn_{1.5}O_4$ Cathode: Improvement on Structure Evolution and Ionic Diffusivity by Chromium Doping. *Journal of Physical Chemistry C* **2018**, *122*, 25229–25236.

25. Arai, H.; Sato, K.; Orikasa, Y.; Murayama, H.; Takahashi, I.; Koyama, Y.; Uchimoto, Y.; Ogumi, Z. Phase transition kinetics of LiNi0.5Mn1.5O4 electrodes studied by in situ X-ray absorption near-edge structure and X-ray diffraction analysis. *Journal of Materials Chemistry A* **2013**, *1*, 10442.

26. Bauer, S.; Biasi, L. d.; Glatthaar, S.; Toukam, L.; Geßwein, H.; Baumbach, T. In operando study of the high voltage spinel cathode material $LiNi_{0.5}Mn_{1.5}O_4$ using two dimensional full-field spectroscopic imaging of Ni and Mn. *Physical Chemistry Chemical Physics* **2015**, *17*, 16388–16397.

27. Kuppan, S.; Xu, Y.; Liu, Y.; Chen, G. Phase transformation mechanism in lithium manganese nickel oxide revealed by single-crystal hard X-ray microscopy. *Nature Communications* **2017**, *8*, 1–10.

28. Liu, H.; Strobridge, F. C.; Borkiewicz, O. J.; Wiaderek, K. M.; Chapman, K. W.; Chupas, P. J.; Grey, C. P. Capturing metastable structures during high-rate cycling of $LiFePO_4$ nanoparticle electrodes. *Science* **2014**, *344*, 1252817.

29. Satou, Y.; Shimonishi, Y.; Komine, S.; Shimizu, S.; Itou, S.; Asai, H. Hysteretic Phenomena between Charging and Discharging in $LiNi_{0.5}Mn_{1.5}O_{4-\sigma}$. *Journal of the Electrochemical Society* **2017**, *164*, A2790–A2793.

30. Konya, T.; Shiramata, Y.; Nakamura, T. Operando XRD study of LiMn1.5Ni0.5O4 high-voltage cathode under high-rate charge-discharge reaction. *Powder Diffraction* **2019**, *34*, S8–S13.

31. Liang, G.; Pillai, A. S.; Peterson, V. K.; Ko, K.-Y.; Chang, C.-M.; Lu, C.-Z.; Liu, C.-E.; Liao, S.-C.; Chen, J.-M.; Guo, Z.; Pang, W. K. Effect of AlF3-Coated Li4Ti5O12 on the Performance and Function of the LiNi0.5Mn1.5O4||Li4Ti5O12 Full Battery—An in-operando Neutron Powder Diffraction Study. *Frontiers in Energy Research* **2018**, *6*, 89.

32. Shimoda, K.; Murakami, M.; Komatsu, H.; Arai, H.; Uchimoto, Y.; Ogumi, Z. Delithiation/Lithiation Behavior of $LiNi_{0.5}Mn_{1.5}O_4$ Studied by In Situ and Ex Situ 6,7 Li NMR Spectroscopy. *The Journal of Physical Chemistry C* **2015**, *119*, 13472–13480.

33. Bianchini, M.; Fauth, F.; Suard, E.; Leriche, J. B.; Masquelier, C.; Croguennec, L. Spinel materials for Li-ion batteries: New insights obtained by operando neutron and synchrotron X-ray diffraction. *Acta Crystallographica Section B: Structural Science, Crystal Engineering and Materials* **2015**, *71*, 688–701.

34. Martinez, S.; Sobrados, I.; Tonti, D.; Amarilla, J. M.; Sanz, J. Chemical vs. electrochemical extraction of lithium from the Li-excess Li1.10Mn1.90O4 spinel followed by NMR and DRX techniques. *Physical Chemistry Chemical Physics* **2014**, *16*, 3282.

35. Amin, R.; Muralidharan, N.; Petla, R. K.; Ben Yahia, H.; Jassim Al-Hail, S. A.; Essehli, R.; Daniel, C.; Khaleel, M. A.; Belharouak, I. Research advances on cobalt-free cathodes for Li-ion batteries - The high voltage LiMn1.5Ni0.5O4 as an example. *Journal of Power Sources* **2020**, *467*, 228318.

36. Drozhzhin, O. A.; Alekseeva, A. M.; Shevchenko, V. A.; Chernyshov, D.; Abakumov, A. M.; Antipov, E. V. Phase Transitions in the "Spinel-Layered" Li1+xNi0.5Mn1.5O4 (x = 0, 0.5, 1) Cathodes upon (De)lithiation Studied with Operando Synchrotron X-ray Powder Diffraction. *Nanomaterials* **2021**, *11*, 1368.

37. Yao, K. P.; Okasinski, J. S.; Kalaga, K.; Shkrob, I. A.; Abraham, D. P. Quantifying lithium concentration gradients in the graphite electrode of Li-ion cells using: Operando energy dispersive X-ray diffraction. *Energy and Environmental Science* **2019**, *12*, 656–665.

38. Finegan, D. P.; Quinn, A.; Wragg, D. S.; Colclasure, A. M.; Lu, X.; Tan, C.; Heenan, T. M.; Jervis, R.; Brett, D. J.; Das, S.; Gao, T.; Cogswell, D. A.; Bazant, M. Z.; Di Michiel, M.; Checchia, S.; Shearing, P. R.; Smith, K. Spatial dynamics of lithiation and lithium plating during high-rate operation of graphite electrodes.

Energy and Environmental Science **2020**, *13*, 2570–2584.

39. Dawkins, J. I.; Ghavidel, M. Z.; Chhin, D.; Beaulieu, I.; Hossain, M. S.; Feng, R.; Mauzeroll, J.; Schougaard, S. B. Operando tracking of solution-phase concentration profiles in Li-ion battery positive electrodes using X-ray fluorescence. *Analytical Chemistry* **2020**, *92*, 10908–10912.

40. Blanco, M. V.; Devaux, D.; Valtavirta, A.-M.; Cosculluela, C.; Watier, Y.; Quazuguel, L.; Deschamps, M.; Lecuyer, M.; Bouchet, R.; Cova, F. Simultaneous Monitoring of Structural Changes and Phase Distribution of LiFePO4 Along the Cathode Thickness of Li Metal Polymer Battery. *Journal of The Electrochemical Society* **2020**, *167*, 160517.

41. Berhaut, C. L.; Dominguez, D. Z.; Kumar, P.; Jouneau, P. H.; Porcher, W.; Aradilla, D.; Tardif, S.; Pouget, S.; Lyonnard, S. Multiscale Multiphase Lithiation and Delithiation Mechanisms in a Composite Electrode Unraveled by Simultaneous Operando Small-Angle and Wide-Angle X-Ray Scattering. *ACS Nano* **2019**, *13*, 11538–11551.

42. Shui, J. L.; Okasinski, J. S.; Kenesei, P.; Dobbs, H. A.; Zhao, D.; Almer, J. D.; Liu, D. J. Reversibility of anodic lithium in rechargeable lithium-oxygen batteries. *Nature Communications* **2013**, *4*, 1–7.

43. Zhang, Y.; Yang, Z.; Tian, C. Probing and quantifying cathode charge heterogeneity in Li ion batteries. *Journal of Materials Chemistry A* **2019**, *7*, 23628–23661.

44. Raimondi, P. ESRF-EBS: The Extremely Brilliant Source Project. *Synchrotron Radiation News* **2016**, *29*, 8–15.

45. Bhatia, A.; Dridi Zrelli, Y.; Pereira-Ramos, J. P.; Baddour-Hadjean, R. Detailed redox mechanism and self-discharge diagnostic of 4.9 V LiMn1.5Ni0.5O4 spinel cathode revealed by Raman spectroscopy.

Journal of Materials Chemistry A **2021**, *9*, 13496–13505.

46. Ma, J.; Hu, P.; Cui, G.; Chen, L. Surface and Interface Issues in Spinel LiNi 0.5 Mn 1.5 O 4 : Insights into a Potential Cathode Material for High Energy Density Lithium Ion Batteries. *Chemistry of Materials* **2016**, *28*, 3578–3606.

47. Xu, Z.; Jiang, Z.; Kuai, C.; Xu, R.; Qin, C.; Zhang, Y.; Rahman, M. M.; Wei, C.; Nordlund, D.; Sun, C. J.; Xiao, X.; Du, X. W.; Zhao, K.; Yan, P.; Liu, Y.; Lin, F. Charge distribution guided by grain crystallographic orientations in polycrystalline battery materials. *Nature Communications* **2020**, *11*, 1–9.

48. Spence, S. L.; Hu, A.; Jiang, M.; Xu, Z.; Yang, Z.; Rahman, M. M.; Li, L.; Chu, Y. S.; Xiao, X.; Huang, X.; Lin, F. Mapping Lattice Distortions in LiNi0.5Mn1.5O4 Cathode Materials. *ACS Energy Letters* **2022**, *7*, 690–695.

49. Uematsu, H.; Ishiguro, N.; Abe, M.; Takazawa, S.; Kang, J.; Hosono, E.; Nguyen, N. D.; Dam, H. C.; Okubo, M.; Takahashi, Y. Visualization of Structural Heterogeneities in Particles of Lithium Nickel Manganese Oxide Cathode Materials by Ptychographic X-ray Absorption Fine Structure. *The Journal of Physical Chemistry Letters* **2021**, *12*, 5781–5788.

50. Gu, Y.-J.; Li, Y.; Chen, Y.-B.; Liu, H.-Q. Comparison of Li/Ni antisite defects in Fd-3 m and P4 3 32 nanostructured LiNi 0.5 Mn 1.5 O 4 electrode for Li-ion batteries. *Electrochimica Acta* **2016**, *213*, 368–374.

51. Lee, E.; Persson, K. A. Revealing the coupled cation interactions behind the electrochemical profile of LixNi0.5Mn1.5O4. *Energy & Environmental Science* **2012**, *5*, 6047.

52. Cogswell, D. A.; Bazant, M. Z. Coherency strain and the kinetics of phase separation in LiFePO 4 nanoparticles. *ACS Nano* **2012**, *6*, 2215–2225.

53. Samarasingha, P. B.; Sottmann, J.; Margadonna, S.; Emerich, H.; Nilsen, O.; Fjellvåg, H. In situ synchrotron study of ordered and disordered LiMn1.5Ni0.5O4 as lithium ion battery positive electrode. *Acta Materialia* **2016**, *116*, 290–297.

54. Qiao, R.; Wang, Y.; Olalde-Velasco, P.; Li, H.; Hu, Y.-S.; Yang, W. Direct evidence of gradient Mn(II) evolution at charged states in LiNi0.5Mn1.5O4 electrodes with capacity fading. *Journal of Power Sources* **2015**, *273*, 1120–1126.

55. Sushko, P. V.; Rosso, K. M.; Zhang, J.-G.; Liu, J.; Sushko, M. L. Oxygen Vacancies and Ordering of d-levels Control Voltage Suppression in Oxide Cathodes: the Case of Spinel LiNi 0.5 Mn 1.5 O 4- δ. *Advanced Functional Materials* **2013**, *23*, 5530–5535.

56. Liu, H.; Kazemiabnavi, S.; Grenier, A.; Vaughan, G.; Di Michiel, M.; Polzin, B. J.; Thornton, K.; Chapman, K. W.; Chupas, P. J. Quantifying Reaction and Rate Heterogeneity in Battery Electrodes in 3D through Operando X-ray Diffraction Computed Tomography. *ACS Applied Materials & Interfaces* **2019**, *11*, 18386–18394.

57. Hua, W.; Wang, S.; Knapp, M.; Leake, S. J.; Senyshyn, A.; Richter, C.; Yavuz, M.; Binder, J. R.; Grey, C. P.; Ehrenberg, H.; Indris, S.; Schwarz, B. Structural insights into the formation and voltage degradation of lithium- and manganese-rich layered oxides. *Nature Communications* **2019**, *10*, 1–11.

58. Tan, C.; Daemi, S. R.; Taiwo, O. O.; Heenan, T. M.; Brett, D. J.; Shearing, P. R. Evolution of electrochemical cell designs for in-situ and operando 3D characterization. *Materials* **2018**, *11*.

59. Borkiewicz, O. J.; Wiaderek, K. M.; Chupas, P. J.; Chapman, K. W. Best practices for operando battery experiments: Influences of X-ray experiment design on observed electrochemical reactivity. *Journal*

of Physical Chemistry Letters **2015**, *6*, 2081–2085.

Graphical TOC Entry